

## Guiding-center Vlasov-Maxwell description of intense beam propagation through a periodic focusing field

Ronald C. Davidson and Hong Qin

*Plasma Physics Laboratory, Princeton University, Princeton, New Jersey 08543*

(Received 6 September 2001; published 24 October 2001)

This paper provides a systematic derivation of a guiding-center kinetic model that describes intense beam propagation through a periodic focusing lattice with axial periodicity length  $S$ , valid for sufficiently small phase advance (say,  $\sigma < 60^\circ$ ). The analysis assumes a thin ( $a, b \ll S$ ) axially continuous beam, or very long charge bunch, propagating in the  $z$  direction through a periodic focusing lattice with transverse focusing coefficients  $\kappa_x(s + S) = \kappa_x(s)$  and  $\kappa_y(s + S) = \kappa_y(s)$ , where  $S = \text{const}$  is the lattice period. By averaging over the (fast) oscillations occurring on the length scale of a lattice period  $S$ , the analysis leads to *smooth-focusing* Vlasov-Maxwell equations that describe the *slow* evolution of the guiding-center distribution function  $\tilde{f}_b(\bar{x}, \bar{y}, \bar{x}', \bar{y}', s)$  and (normalized) self-field potential  $\tilde{\psi}(\bar{x}, \bar{y}, s)$  in the four-dimensional transverse phase space  $(\bar{x}, \bar{y}, \bar{x}', \bar{y}')$ . In the resulting kinetic equation for  $\tilde{f}_b(\bar{x}, \bar{y}, \bar{x}', \bar{y}', s)$ , the average effects of the applied focusing field are incorporated in *constant* focusing coefficients  $\kappa_{x, \text{sf}} > 0$  and  $\kappa_{y, \text{sf}} > 0$ , and the model is readily accessible to direct analytical investigation. Similar smooth-focusing Vlasov-Maxwell descriptions are widely used in the accelerator physics literature, often without a systematic justification, and the present analysis is intended to place these models on a rigorous, yet physically intuitive, foundation.

DOI: 10.1103/PhysRevSTAB.4.104401

PACS numbers: 29.27.Bd, 41.75.-i, 41.85.-p

### I. INTRODUCTION

Periodic focusing accelerators and transport systems [1–9] have a wide range of applications ranging from basic scientific research in high energy and nuclear physics to applications such as coherent radiation sources, heavy ion fusion, tritium production, nuclear waste transmutation, and spallation neutron sources for materials and biological research [10,11]. At the high beam currents and charge densities of practical interest, of particular importance are the effects of the intense self-fields produced by the beam space charge and current on determining the detailed equilibrium, stability and transport properties, and the nonlinear dynamics of the system. Through analytical studies based on the nonlinear Vlasov-Maxwell equations for the distribution function  $f_b(\mathbf{x}, \mathbf{p}, t)$  and the self-generated electric and magnetic fields  $\mathbf{E}^s(\mathbf{x}, t)$  and  $\mathbf{B}^s(\mathbf{x}, t)$ , and numerical simulations using particle-in-cell models and nonlinear perturbative simulation techniques, considerable progress has been made in developing an improved understanding of the collective processes and nonlinear beam dynamics characteristic of high-intensity beam propagation in periodic focusing and uniform focusing transport systems [1,12–38]. Theoretical progress has also been made in the development and application of macroscopic fluid models for the description of intense beam equilibrium and stability properties [39–42]. Nonetheless, given the complexity of a detailed description of intense beam propagation based on the nonlinear Vlasov-Maxwell equations, it remains important to develop simplified kinetic models of beam propagation through periodic focusing systems, particularly models which are analyti-

cally tractable and robust in describing beam propagation over large distances. The purpose of this article is to provide a systematic derivation of a guiding-center kinetic model that describes intense beam propagation through a periodic focusing lattice with period  $S$ , valid for sufficiently small phase advance (say,  $\sigma < 60^\circ$ ). By averaging over the (fast) oscillations occurring on the length scale of a lattice period  $S$ , the analysis leads to smooth-focusing Vlasov-Maxwell equations describing the slow evolution of the guiding-center distribution function  $\tilde{f}_b(\bar{x}, \bar{y}, \bar{x}', \bar{y}', s)$  and (normalized) self-field potential  $\tilde{\psi}(\bar{x}, \bar{y}, s)$  in the four-dimensional transverse phase space  $(\bar{x}, \bar{y}, \bar{x}', \bar{y}')$ .

To briefly summarize, we consider a thin ( $a, b \ll S$ ) axially continuous beam (or very long charge bunch) propagating in the  $z$  direction through a periodic focusing lattice with transverse focusing coefficients  $\kappa_x(s + S) = \kappa_x(s)$  and  $\kappa_y(s + S) = \kappa_y(s)$ , where  $S = \text{const}$  is the axial periodicity length. The theoretical model describing the evolution of the distribution function  $f_b(x, y, x', y', s)$  and (normalized) self-field potential  $\psi(x, y, s)$  in the four-dimensional transverse phase space  $(x, y, x', y')$  is summarized in Sec. II. Here,  $x' = dx/ds$  and  $y' = dy/ds$  denote dimensionless transverse velocities. Assuming slow axial variations ( $\lambda_x, \lambda_y \gg S$ ) of the average transverse particle orbits, in Sec. III we derive approximate equations describing the slow evolution of the guiding-center trajectories  $\bar{x}(s)$  and  $\bar{y}(s)$ . The corresponding Hamiltonian  $H_\perp(\bar{x}, \bar{y}, \bar{x}', \bar{y}', s)$  defined in Eq. (54) for the transverse guiding-center motion is then used in Sec. IV to obtain the corresponding Vlasov-Maxwell equations [(57) and (58)] for the guiding-center distribution function

$\bar{f}_b(\bar{x}, \bar{y}, \bar{x}', \bar{y}', s)$  and self-field potential  $\bar{\psi}(\bar{x}, \bar{y}, s)$ . Properties of the guiding-center kinetic equations are summarized in Sec. IV, and the range of validity of the guiding-center model is examined in Sec. V.

In the guiding-center Hamiltonian defined in Eq. (54) and the corresponding Vlasov-Maxwell equations [(57) and (58)], note that the average effects of the applied focusing field are incorporated in the constant coefficients  $\kappa_{x\text{sf}} > 0$  and  $\kappa_{y\text{sf}} > 0$ . While smooth-focusing Vlasov-Maxwell equations similar to Eqs. (57) and (58) are widely used in the accelerator physics literature [14], often without a systematic justification, a primary purpose of this paper is to place Eqs. (57) and (58) on a rigorous, yet physically intuitive, foundation.

## II. THEORETICAL MODEL AND ASSUMPTIONS

In the present analysis, we consider an axial continuous intense charged particle beam (or very long charge bunch) made up of particles with charge  $e_b$  and rest mass  $m_b$  propagating in the  $z$  direction with average axial velocity  $V_b = \beta_b c = \text{const}$  and characteristic directed kinetic energy  $(\gamma_b - 1)m_b c^2$ . Here,  $c$  is the speed of light *in vacuo*,  $\gamma_b = (1 - \beta_b^2)^{-1/2}$  is the relativistic mass factor, and the beam propagates through a periodic focusing lattice with axial periodicity length  $S = \text{const}$ . A perfectly conducting cylindrical wall is located at radius  $r = (x^2 + y^2)^{1/2} = r_w = \text{const}$ . Furthermore, the particle motion in the beam frame is assumed to be nonrelativistic, the axial momentum spread of the beam particles is treated as negligibly small, and the beam is assumed to be *thin*, with characteristic transverse dimensions  $a$  and  $b$  in the  $x$  and  $y$  directions satisfying

$$a, b \ll S. \quad (1)$$

Consistent with the paraxial approximation, it is also assumed that the self-field perveance  $K_b$  satisfies [1]

$$K_b \equiv \frac{2N_b e_b^2}{\gamma_b^3 m_b \beta_b^2 c^2} \ll 1. \quad (2)$$

Here,  $N_b = \int dx dy dx' dy' f_b(x, y, x', y', s)$  is the number of beam particles per unit axial length,  $f_b(x, y, x', y', s)$  is the distribution of particles in the transverse phase space  $(x, y, x', y')$ , and  $s$  is an effective axial coordinate which plays the role of a scaled time variable ( $s = s_0 + \beta_b ct$ ) moving with a beam particle. Finally, assuming a thin beam with  $a, b \ll S$ , we take the applied focusing force on a beam particle to be of the form [1]

$$F_{\text{foc}} = -[\kappa_x(s)x\hat{\mathbf{e}}_x + \kappa_y(s)y\hat{\mathbf{e}}_y], \quad (3)$$

where  $x, y$  is the transverse displacement from the beam axis, and the  $s$ -dependent lattice coefficients correspond to a periodic focusing field configuration with

$$\kappa_x(s + S) = \kappa_x(s), \quad \kappa_y(s + S) = \kappa_y(s). \quad (4)$$

Here,  $S = \text{const}$  is the periodicity length of the focusing lattice. In the thin-beam approximation, note from Eq. (3) that the  $x$  and  $y$  components of the applied focusing force are linearly proportional to  $x$  and  $y$ , respectively, over the beam cross section.

It is convenient to introduce the (dimensionless) self-field potential  $\psi(x, y, s)$  defined by [1]

$$\psi(x, y, s) = \frac{e_b \phi(x, y, s)}{\gamma_b^3 m_b \beta_b^2 c^2}, \quad (5)$$

where  $\phi(x, y, s)$  is the space-charge potential determined self-consistently in terms of the number density of beam particles,  $n_b(x, y, s) = \int dx' dy' f_b(x, y, x', y', s)$ , from Poisson's equation. Consistent with the assumptions enumerated above, the (dimensionless) Hamiltonian  $H_{\perp}(x, y, s', y', s)$ , normalized to  $\gamma_b m_b \beta_b^2 c^2$ , for transverse particle motion in the applied field plus self-generated field configuration is given by [43]

$$H_{\perp} = \frac{1}{2}(x'^2 + y'^2) + \frac{1}{2}[\kappa_x(s)x^2 + \kappa_y(s)y^2] + \psi(x, y, s). \quad (6)$$

As noted earlier, the beam particles are assumed to have a negligibly small spread in axial momentum about the average value  $\gamma_b m_b \beta_b c$ . Then in transverse phase-space variables  $(x, y, x', y')$ , it is readily shown that the distribution function  $f_b(x, y, x', y', s)$  evolves according to the nonlinear Vlasov equation [43]

$$\begin{aligned} \frac{\partial f_b}{\partial s} + x' \frac{\partial f_b}{\partial x} + y' \frac{\partial f_b}{\partial y} - \\ \left( \kappa_x(s)x + \frac{\partial \psi}{\partial x} \right) \frac{\partial f_b}{\partial x'} - \\ \left( \kappa_y(s)y + \frac{\partial \psi}{\partial y} \right) \frac{\partial f_b}{\partial y'} = 0. \end{aligned} \quad (7)$$

Here, the normalized self-field potential  $\psi(x, y, s)$  is determined self-consistently from

$$\left( \frac{\partial^2}{\partial x^2} + \frac{\partial^2}{\partial y^2} \right) \psi = -\frac{2\pi K_b}{N_b} \int dx' dy' f_b. \quad (8)$$

In Eq. (8), the self-field perveance  $K_b$  is defined in Eq. (2),  $n_b(x, y, s) = \int dx' dy' f_b$  is the number density of beam particles, and  $N_b = \int dx dy n_b(x, y, s)$  is the number of beam particles per unit axial length. In Eq. (7) the quantities  $x'$  and  $y'$  correspond to normalized velocity variables in the  $x$ - $y$  plane (i.e.,  $x'$  denotes  $dx/ds$  and  $y'$  denotes  $dy/ds$ ). In addition, the coefficients of  $\partial f_b/\partial x'$  and  $\partial f_b/\partial y'$  correspond to the transverse accelerations,  $dx'/ds = -\partial H_{\perp}/\partial x$  and  $dy'/ds = -\partial H_{\perp}/\partial y$ , respectively. Assuming a perfectly conducting cylindrical wall located at radius  $r = (x^2 + y^2)^{1/2} = r_w$ , Eqs. (7) and (8) are to be solved subject to the boundary condition

$$\left[ \frac{1}{r} \frac{\partial \psi(r, \theta)}{\partial \theta} \right]_{r=r_w} = 0, \quad (9)$$

which corresponds to zero tangential electric field at the conducting wall, i.e.,  $[E_\theta]_{r=r_w} = -[r^{-1}\partial\phi/\partial\theta]_{r=r_w} = 0$ . Here,  $(r, \theta)$  corresponds to cylindrical polar coordinates defined by  $x = r \cos\theta$  and  $y = r \sin\theta$ .

There are two classes of periodic focusing lattices of practical interest. For the first class, the average of the (oscillatory) lattice coefficients  $\kappa_x(s)$  and  $\kappa_y(s)$  over one lattice period  $S$  is equal to zero, i.e.,

$$\int_{s_0}^{s_0+S} ds \kappa_x(s) = 0 = \int_{s_0}^{s_0+S} ds \kappa_y(s). \quad (10)$$

An example of a lattice satisfying Eq. (10) corresponds to a periodic focusing quadrupole field, with  $\mathbf{B}_q = B'_q(z)(y\hat{\mathbf{e}}_x + x\hat{\mathbf{e}}_y)$ , with coupling coefficients defined by [1]

$$\kappa_x(s) = -\kappa_y(s) \equiv \kappa_q(s) = \frac{e_b B'_q(s)}{\gamma_b m_b \beta_b c^2}. \quad (11)$$

Here,  $B'_q(s) \equiv (\partial B_x^q/\partial y)_{(0,0)} = (\partial B_y^q/\partial x)_{(0,0)}$ , and  $\kappa_q(s)$  satisfies

$$\kappa_q(s + S) = \kappa_q(s), \quad \int_{s_0}^{s_0+S} ds \kappa_q(s) = 0, \quad (12)$$

where  $S$  is the axial periodicity length. For the example in Eqs. (11) and (12), note that  $\kappa_x(s)$  and  $\kappa_y(s)$  have the same magnitudes but opposite signs, and oscillate about zero average value. That is, the force exerted by the applied quadrupole field is alternately focusing and defocusing.

As a second example, we consider a periodic focusing solenoidal field,  $\mathbf{B}_{\text{sol}} = B_z(z)\hat{\mathbf{e}}_z - (1/2)B'_z(z)(x\hat{\mathbf{e}}_x + y\hat{\mathbf{e}}_y)$ , where  $B'_z(z) = (\partial B_z^{\text{sol}}/\partial z)_{(0,0)}$ . In this case, in Larmor frame variables, the Hamiltonian and nonlinear Vlasov-Maxwell equations are identical in form to Eqs. (6)–(8), and the lattice coefficients  $\kappa_x(s)$  and  $\kappa_y(s)$  satisfy [1]

$$\kappa_x(s) = \kappa_y(s) \equiv \kappa_z(s) = \left( \frac{e_b B_z(s)}{2\gamma_b m_b \beta_b c^2} \right)^2, \quad (13)$$

where

$$\kappa_z(s + S) = \kappa_z(s). \quad (14)$$

Note from Eq. (13) that  $\kappa_x(s)$  and  $\kappa_y(s)$  have the same magnitudes and (positive) sign, and the force exerted by the applied solenoidal field is always focusing. We denote the average of an  $s$ -dependent function over one lattice period  $S$  by

$$\langle \dots \rangle = \frac{1}{S} \int_{s_0}^{s_0+S} ds \dots \quad (15)$$

Denoting  $\bar{\kappa}_x = \langle \kappa_x(s) \rangle$ ,  $\bar{\kappa}_y = \langle \kappa_y(s) \rangle$ , etc., it follows from Eq. (13) that

$$\bar{\kappa}_x = \bar{\kappa}_y = \bar{\kappa}_z, \quad (16)$$

where

$$\bar{\kappa}_z = \frac{1}{S} \int_{s_0}^{s_0+S} ds \kappa_z(s), \quad (17)$$

and  $\bar{\kappa}_z > 0$ .

In concluding this section, we have provided two examples of periodic focusing field configurations. One example corresponds to a periodic focusing quadrupole lattice in which the average of the lattice coefficients  $\kappa_x(s)$  and  $\kappa_y(s)$  over one lattice period  $S$  is equal to zero [Eqs. (10)–(12)]. The second example corresponds to a periodic focusing solenoidal field in which the average of the lattice coefficients  $\kappa_x(s)$  and  $\kappa_y(s)$  over one lattice period  $S$  is nonzero [Eqs. (13)–(17)]. It is important to keep in mind that the guiding-center formalism developed in Sec. III is applicable to both classes of field configurations.

### III. GUIDING-CENTER ORBIT EQUATIONS

We now return to the nonlinear Vlasov-Maxwell equations (7) and (8) and the Hamiltonian  $H_\perp(x, y, x', y', s)$  defined in Eq. (6) for the particle motion in the transverse phase space  $(x, y, x', y')$ . The characteristics of the nonlinear Vlasov equation (7), of course, correspond to the equations of motion determined from

$$\begin{aligned} \frac{dx}{ds} &= \frac{\partial H_\perp}{\partial x'}, & \frac{dx'}{ds} &= -\frac{\partial H_\perp}{\partial x}, \\ \frac{dy}{ds} &= \frac{\partial H_\perp}{\partial y'}, & \frac{dy'}{ds} &= -\frac{\partial H_\perp}{\partial y}, \end{aligned} \quad (18)$$

where  $x' = dx/ds$  and  $y' = dy/ds$ . Substituting Eq. (6) into Eq. (18) readily gives the familiar equations of motion for the transverse orbits  $x(s)$  and  $y(s)$ . We obtain

$$\frac{d^2x}{ds^2} + \kappa_x(s)x = -\frac{\partial}{\partial x} \psi(x, y, s), \quad (19)$$

$$\frac{d^2y}{ds^2} + \kappa_y(s)y = -\frac{\partial}{\partial y} \psi(x, y, s), \quad (20)$$

where the self-field potential  $\psi(x, y, s)$  is determined self-consistently from Poisson's equation (8). The acceleration terms proportional to  $-\kappa_x(s)x$  and  $-\kappa_y(s)y$  in Eqs. (19) and (20) describe the focusing and defocusing effects of the applied field configuration, whereas the terms proportional to  $-\partial\psi/\partial x$  and  $-\partial\psi/\partial y$  describe the acceleration components due to self-field effects. Using the method of characteristics [1], solving the nonlinear orbit equations (19) and (20) is fully equivalent to solving the nonlinear Vlasov-Maxwell equations (7) and (8).

A detailed analysis of Eqs. (19) and (20) for the general self-field potential  $\psi(x, y, s)$  and corresponding self-consistent distribution function  $f_b(x, y, x', y', s)$  is difficult, except in the context of ancillary simplifying assumptions. The purpose of this article is to describe one such case of considerable practical interest in which simplification occurs. In the present analysis, we consider circumstances in which the phase advance is sufficiently

small (say,  $\sigma < 2\pi/6 = 60^\circ$ ) that the *average orbits* for  $x(s)$  and  $y(s)$  are slowly varying over one lattice period  $S$ . In particular, we express

$$x(s) = \bar{x} + \delta x(s), \quad y(s) = \bar{y} + \delta y(s), \quad (21)$$

where

$$\langle \delta x \rangle = 0 = \langle \delta y \rangle, \quad (22)$$

and  $\bar{x}(s)$  and  $\bar{y}(s)$  are slowly varying functions of  $s$ . Here,  $(\bar{x}, \bar{y})$  is referred to as the *guiding center* of the transverse particle orbits, and  $\langle \dots \rangle = S^{-1} \int_{s_0}^{s_0+S} ds \dots$  denotes an average over one lattice period  $S$ . Here the terminology ‘‘guiding-center’’ orbit refers to the *average* orbit of a particle, where averages are taken over the (rapid) oscillations of the focusing lattice.

In Eq. (21), the (rapid) oscillatory modulation of  $\delta x(s)$  and  $\delta y(s)$  occurs on the length scale  $S$ , whereas the characteristic length scales for the (slow) changes in  $\bar{x}(s)$  and  $\bar{y}(s)$ , which we denote by  $\lambda_x$  and  $\lambda_y$ , are assumed to be much larger than the lattice period  $S$ , i.e.,

$$S \ll \lambda_x, \lambda_y. \quad (23)$$

In the subsequent analysis, we will show [see Eqs. (46) and (47)] that the average applied forces acting on the guiding-center orbits  $\bar{x}$  and  $\bar{y}$  are proportional to  $-\kappa_{x\text{sf}}\bar{x}$  and  $-\kappa_{y\text{sf}}\bar{y}$ , respectively, where  $\kappa_{x\text{sf}} > 0$  and  $\kappa_{y\text{sf}} > 0$  are positive (smooth-focusing) lattice coefficients [36] which always correspond to an inward focusing force on the guiding-center orbits. In this case, we estimate  $\lambda_x \sim 2\pi/\sqrt{\kappa_{x\text{sf}}}$  and  $\lambda_y \sim 2\pi/\sqrt{\kappa_{y\text{sf}}}$  so that Eq. (23) is equivalent to the requirement

$$\frac{\sqrt{\kappa_{x\text{sf}}} S}{2\pi}, \frac{\sqrt{\kappa_{y\text{sf}}} S}{2\pi} \sim \Delta < 1, \quad (24)$$

where  $\Delta$  is a small dimensionless parameter. Note that the inequality in Eq. (24) corresponds to a transverse focusing field with sufficiently low intensity (sufficiently small phase advance).

We now return to the orbit equations (19) and (20) and express

$$\kappa_x(s) = \bar{\kappa}_x + \delta\kappa_x(s), \quad \kappa_y(s) = \bar{\kappa}_y + \delta\kappa_y(s), \quad (25)$$

where  $\bar{\kappa}_x \equiv S^{-1} \int_{s_0}^{s_0+S} ds \kappa_x(s)$  and  $\bar{\kappa}_y \equiv S^{-1} \int_{s_0}^{s_0+S} ds \kappa_y(s)$ , and  $\delta\kappa_x(s+S) = \delta\kappa_x(s)$  and  $\delta\kappa_y(s+S) = \delta\kappa_y(s)$  follow from Eq. (4). The averages of  $\delta\kappa_x(s)$  and  $\delta\kappa_y(s)$  over one lattice period are, of course, equal to zero, i.e.,

$$\langle \delta\kappa_x(s) \rangle = 0 = \langle \delta\kappa_y(s) \rangle, \quad (26)$$

where  $\langle \dots \rangle = S^{-1} \int_{s_0}^{s_0+S} ds \dots$ . In the subsequent analysis of Eqs. (19) and (20) we generally allow for nonzero values of the constants  $\bar{\kappa}_x$  and  $\bar{\kappa}_y$ , although for the particular case of a periodic focusing quadrupole field described by Eqs. (11) and (12), it follows that  $\bar{\kappa}_x = 0 = \bar{\kappa}_y$ . Substituting Eqs. (21) and (25) into the orbit equations (19) and (20), we obtain

$$\begin{aligned} \frac{d^2}{ds^2} (\bar{x} + \delta x) + [\bar{\kappa}_x + \delta\kappa_x(s)] (\bar{x} + \delta x) \\ = -\frac{\partial}{\partial \bar{x}} \psi(\bar{x} + \delta x, \bar{y} + \delta y, s), \end{aligned} \quad (27)$$

$$\begin{aligned} \frac{d^2}{ds^2} (\bar{y} + \delta y) + [\bar{\kappa}_y + \delta\kappa_y(s)] (\bar{y} + \delta y) \\ = -\frac{\partial}{\partial \bar{y}} \psi(\bar{x} + \delta x, \bar{y} + \delta y, s). \end{aligned} \quad (28)$$

In the analysis of Eqs. (27) and (28), we formally treat the  $\kappa_x$ ,  $\kappa_y$ , and  $\psi$  terms to all be of order  $\Delta$ , i.e.,

$$\kappa_x \sim \kappa_y \sim \psi = O(\Delta). \quad (29)$$

In addition, the excursions  $(\delta x, \delta y)$  about the guiding-center orbit  $(\bar{x}, \bar{y})$  are also assumed to be of order  $\Delta$ , i.e.,

$$\delta x \sim \delta y = O(\Delta). \quad (30)$$

From Eq. (29), note that the self-field potential is allowed to be comparable in size to the applied focusing field. This corresponds to a *maximal ordering* which is valid for high beam intensity. Such an analysis automatically includes the case of low-to-moderate beam intensity, where  $\psi = O(\Delta^2)$ , say.

Next we make use of Eqs. (29) and (30) to Taylor expand the right-hand sides of Eqs. (27) and (28), formally retaining terms to order  $\Delta^2$ . This gives the (approximate) orbit equations

$$\begin{aligned} \frac{d^2}{ds^2} (\bar{x} + \delta x) + [\bar{\kappa}_x + \delta\kappa_x(s)] (\bar{x} + \delta x) \\ = -\frac{\partial}{\partial \bar{x}} [\bar{\psi}(\bar{x}, \bar{y}, s) + \delta\psi(\bar{x}, \bar{y}, s)] - \left[ \delta x \frac{\partial^2}{\partial \bar{x}^2} + \delta y \frac{\partial^2}{\partial \bar{y} \partial \bar{x}} \right] \bar{\psi}(\bar{x}, \bar{y}, s) + \dots, \end{aligned} \quad (31)$$

$$\begin{aligned} \frac{d^2}{ds^2} (\bar{y} + \delta y) + [\bar{\kappa}_y + \delta\kappa_y(s)] (\bar{y} + \delta y) \\ = -\frac{\partial}{\partial \bar{y}} [\bar{\psi}(\bar{x}, \bar{y}, s) + \delta\psi(\bar{x}, \bar{y}, s)] - \left[ \delta y \frac{\partial^2}{\partial \bar{y}^2} + \delta x \frac{\partial^2}{\partial \bar{x} \partial \bar{y}} \right] \bar{\psi}(\bar{x}, \bar{y}, s) + \dots. \end{aligned} \quad (32)$$

In Eqs. (31) and (32), we expressed  $\psi(\bar{x}, \bar{y}, s) = \bar{\psi}(\bar{x}, \bar{y}, s) + \delta\psi(\bar{x}, \bar{y}, s)$ , where  $\bar{\psi}(\bar{x}, \bar{y}, s)$  is a slowly varying function of  $s$ , and the rapid oscillations are incorporated in  $\delta\psi(\bar{x}, \bar{y}, s)$  with  $\langle \delta\psi \rangle = (1/S) \int_{s_0}^{s_0+S} ds \delta\psi(\bar{x}, \bar{y}, s) = 0$ . Equations (31) and (32) can be used to obtain equations for the (slow) evolution of the guiding-center orbits  $\bar{x}$  and  $\bar{y}$ . We assume that  $\bar{\psi}(\bar{x}, \bar{y}, s)$  is a slowly varying function of  $s$ , and make use of  $\langle \delta\kappa_x \rangle = 0 = \langle \delta\kappa_y \rangle$  [Eq. (26)] and  $\langle \delta x \rangle = 0 = \langle \delta y \rangle$  [Eq. (22)]. Operating on Eqs. (31) and (32) with  $S^{-1} \int_{s_0}^{s_0+S} \dots$  then gives

$$\frac{d^2 \bar{x}}{ds^2} + \bar{\kappa}_x \bar{x} + \langle \delta\kappa_x(s) \delta x(s) \rangle = -\frac{\partial}{\partial \bar{x}} \bar{\psi}(\bar{x}, \bar{y}, s), \quad (33)$$

$$\frac{d^2 \bar{y}}{ds^2} + \bar{\kappa}_y \bar{y} + \langle \delta\kappa_y(s) \delta y(s) \rangle = -\frac{\partial}{\partial \bar{y}} \bar{\psi}(\bar{x}, \bar{y}, s), \quad (34)$$

where the average  $\langle \dots \rangle$  is defined in Eq. (15). In obtaining Eqs. (33) and (34), it was assumed that  $\delta x(s+S) = \delta x(s)$  and  $\delta y(s+S) = \delta y(s)$ , so that  $\langle d^2 \delta x/ds^2 \rangle = 0 = \langle d^2 \delta y/ds^2 \rangle$  when averaged over one lattice period. Subtracting Eqs. (33) and (34) from Eqs. (31) and (32), respectively, then gives for the evolution of  $\delta x(s)$  and  $\delta y(s)$

$$\frac{d^2 \delta x}{ds^2} + \delta\kappa_x(s) \bar{x} = \langle \delta\kappa_x(s) \delta x(s) \rangle - [\bar{\kappa}_x + \delta\kappa_x(s)] \delta x - \frac{\partial}{\partial \bar{x}} \delta\psi(\bar{x}, \bar{y}, s) - \left[ \delta x \frac{\partial^2}{\partial \bar{x}^2} + \delta y \frac{\partial^2}{\partial \bar{y} \partial \bar{x}} \right] \bar{\psi}(\bar{x}, \bar{y}, s), \quad (35)$$

$$\frac{d^2 \delta y}{ds^2} + \delta\kappa_y(s) \bar{y} = \langle \delta\kappa_y(s) \delta y(s) \rangle - [\bar{\kappa}_y + \delta\kappa_y(s)] \delta y - \frac{\partial}{\partial \bar{y}} \delta\psi(\bar{x}, \bar{y}, s) - \left[ \delta y \frac{\partial^2}{\partial \bar{y}^2} + \delta x \frac{\partial^2}{\partial \bar{x} \partial \bar{y}} \right] \bar{\psi}(\bar{x}, \bar{y}, s), \quad (36)$$

correct to order  $\Delta^2$ . Note that the terms proportional to  $\delta\kappa_x(s) \bar{x}$  and  $\delta\kappa_y(s) \bar{y}$  in Eqs. (35) and (36) are formally of order  $\Delta$ , whereas the terms on the right-hand side of Eqs. (35) and (36) are proportional to  $\kappa_x \delta x$ ,  $\delta x \bar{\psi}$ ,  $\delta\psi$ ,  $\delta y \bar{\psi}$ , and  $\kappa_y \delta y$ , which are of order  $\Delta^2$  [Eqs. (29) and (30)]. Therefore, in leading order, we approximate Eqs. (35) and (36) by

$$\frac{d^2}{ds^2} \delta x(s) + \delta\kappa_x(s) \bar{x} = 0, \quad (37)$$

$$\frac{d^2}{ds^2} \delta y(s) + \delta\kappa_y(s) \bar{y} = 0, \quad (38)$$

to the level of accuracy required to calculate the averages  $\langle \delta\kappa_x \delta x \rangle$  and  $\langle \delta\kappa_y \delta y \rangle$  in the guiding-center orbit equations for  $\bar{x}$  and  $\bar{y}$  in Eqs. (33) and (34).

We now return to Eqs. (33) and (34) to simplify the expressions for  $\langle \delta\kappa_x \delta x \rangle$  and  $\langle \delta\kappa_y \delta y \rangle$ . For example, some straightforward algebra shows that

$$\langle \delta\kappa_x(s) \delta x(s) \rangle = \left\langle \left( \frac{d}{ds} \int_{s_0}^s ds \delta\kappa_x(s) \right) \delta x(s) \right\rangle = - \left\langle \left( \int_{s_0}^s ds \delta\kappa_x(s) \right) \frac{d}{ds} \delta x(s) \right\rangle, \quad (39)$$

where we have integrated by parts with respect to  $s$  and made use of  $\int_{s_0}^{s_0+S} ds \delta\kappa_x(s) = 0$  [Eq. (26)]. Integrating Eq. (37) once with respect to  $s$  then gives

$$\frac{d}{ds} \delta x(s) = \frac{d}{ds} \delta x \Big|_{s=s_0} - \bar{x} \int_{s_0}^s ds \delta\kappa_x(s). \quad (40)$$

Substituting Eq. (40) into Eq. (39), we obtain

$$\langle \delta\kappa_x(s) \delta x(s) \rangle = \left\langle \left( \int_{s_0}^s ds \delta\kappa_x(s) \right)^2 \right\rangle \bar{x} - \left\langle \int_{s_0}^s ds \delta\kappa_x(s) \right\rangle \frac{d}{ds} \delta x \Big|_{s=s_0}. \quad (41)$$

The factor  $[d\delta x/ds]_{s=s_0}$  occurring in Eq. (41) can be eliminated by making use of Eq. (40). Operating on Eq. (40) with  $S^{-1} \int_{s_0}^{s_0+S} ds \dots$ , and making use of  $\langle (d/ds) \delta x(s) \rangle = 0$ , readily gives  $[d\delta x/ds]_{s=s_0} = \bar{x} \langle \int_{s_0}^s ds \delta\kappa_x(s) \rangle$ . Substituting into Eq. (41) then gives the compact result

$$\langle \delta\kappa_x(s) \delta x(s) \rangle = \left[ \left\langle \left( \int_{s_0}^s ds \delta\kappa_x(s) \right)^2 \right\rangle - \left\langle \int_{s_0}^s ds \delta\kappa_x(s) \right\rangle^2 \right] \bar{x} = \left\langle \left( \int_{s_0}^s ds \delta\kappa_x(s) - \left\langle \int_{s_0}^s ds \delta\kappa_x(s) \right\rangle \right)^2 \right\rangle \bar{x}. \quad (42)$$

In a completely analogous manner, it can be shown from Eq. (38) that

$$\langle \delta\kappa_y(s) \delta y(s) \rangle = \left[ \left\langle \left( \int_{s_0}^s ds \delta\kappa_y(s) \right)^2 \right\rangle - \left\langle \int_{s_0}^s ds \delta\kappa_y(s) \right\rangle^2 \right] \bar{y} = \left\langle \left( \int_{s_0}^s ds \delta\kappa_y(s) - \left\langle \int_{s_0}^s ds \delta\kappa_y(s) \right\rangle \right)^2 \right\rangle \bar{y}. \quad (43)$$

Equations (42) and (43) constitute the final expressions for  $\langle \delta \kappa_x \delta x \rangle$  and  $\langle \delta \kappa_y \delta y \rangle$  required in Eqs. (33) and (34) for the guiding-center orbits  $\bar{x}$  and  $\bar{y}$ . In this regard, we introduce the ( $s$ -independent) smooth-focusing coefficients  $\kappa_{x\text{sf}}$  and  $\kappa_{y\text{sf}}$  defined by

$$\kappa_{x\text{sf}} \equiv \bar{\kappa}_x + \left\langle \left( \int_{s_0}^s ds \delta \kappa_x(s) - \left\langle \int_{s_0}^s ds \delta \kappa_x(s) \right\rangle \right)^2 \right\rangle, \quad (44)$$

$$\kappa_{y\text{sf}} \equiv \bar{\kappa}_y + \left\langle \left( \int_{s_0}^s ds \delta \kappa_y(s) - \left\langle \int_{s_0}^s ds \delta \kappa_y(s) \right\rangle \right)^2 \right\rangle. \quad (45)$$

Making use of Eqs. (42)–(45), the orbit equations [(33) and (34)] describing the slow evolution of the guiding-center orbits  $\bar{x}(s)$  and  $\bar{y}(s)$  can be expressed as

$$\frac{d^2 \bar{x}}{ds^2} + \kappa_{x\text{sf}} \bar{x} = -\frac{\partial}{\partial \bar{x}} \bar{\psi}(\bar{x}, \bar{y}, s), \quad (46)$$

$$\frac{d^2 \bar{y}}{ds^2} + \kappa_{y\text{sf}} \bar{y} = -\frac{\partial}{\partial \bar{y}} \bar{\psi}(\bar{x}, \bar{y}, s), \quad (47)$$

where  $\kappa_{x\text{sf}}$  and  $\kappa_{y\text{sf}}$  are the positive constants defined in Eqs. (44) and (45).

Equations (46) and (47) constitute the final dynamical equations for the guiding-center orbits  $\bar{x}$  and  $\bar{y}$  correct to leading order in the small parameter  $\Delta$  [Eq. (24)]. Several features of Eqs. (46) and (47) are noteworthy. First, because  $\kappa_{x\text{sf}} > 0$  and  $\kappa_{y\text{sf}} > 0$ , the applied-force terms in Eqs. (46) and (47) are always focusing. Second, because  $\kappa_{x\text{sf}}$  and  $\kappa_{y\text{sf}}$  are constants (independent of  $s$ ), an analysis of Eqs. (46) and (47) for the guiding-center orbits is considerably more straightforward than an analysis of Eqs. (19) and (20) for the exact trajectories  $x(s)$  and  $y(s)$ . Indeed, in Eqs. (19) and (20), the focusing coefficients  $\kappa_x(s)$  and  $\kappa_y(s)$  are rapidly varying functions of  $s$ , which makes a detailed analysis of Eqs. (19) and (20) considerably more difficult. Furthermore, the terms proportional to  $-\partial \bar{\psi} / \partial \bar{x}$  and  $-\partial \bar{\psi} / \partial \bar{y}$  in Eqs. (46) and (47) describe the important influence of the average self-fields generated by the beam space charge and axial current on the evolution of the guiding-center orbits  $\bar{x}$  and  $\bar{y}$ . That is, no *a priori* assumption that the beam intensity is low and that self-field effects are correspondingly weak has been made in the derivation of Eqs. (46) and (47). As a consequence, Eqs. (46) and (47) can be used to investigate the guiding-center dynamics for a broad range of guiding-center distributions  $\bar{f}_b(\bar{x}, \bar{y}, \bar{x}', \bar{y}', s)$  and corresponding self-field potential  $\bar{\psi}(\bar{x}, \bar{y}, s)$ . Finally, it is evident from Eqs. (46) and (47) that the characteristic oscillation wavelengths in  $\bar{x}$  and  $\bar{y}$  induced by the average effects of the applied focusing field are  $\lambda_x \sim 2\pi / \sqrt{\kappa_{x\text{sf}}}$  and  $\lambda_y \sim 2\pi / \sqrt{\kappa_{y\text{sf}}}$ . Therefore, the assumption that the lattice period  $S$  satisfies  $S \ll \lambda_x, \lambda_y$  in the derivation of Eqs. (46) and (47) is equivalent to the inequality assumed in Eq. (24).

An important feature of the present analysis is that, at sufficiently high beam intensity, the self-field terms in Eqs. (46) and (47) become increasingly important, and the phase advance is further depressed relative to the vacuum estimates  $\lambda_x \sim 2\pi / \sqrt{\kappa_{x\text{sf}}}$  and  $\lambda_y \sim 2\pi / \sqrt{\kappa_{y\text{sf}}}$ .

In concluding this section, we emphasize that the analysis leading to the guiding-center orbit equations (46) and (47) is valid for a wide range of choices of lattice functions with periodic waveform,  $\kappa_x(s + S) = \kappa_x(s)$  and  $\kappa_y(s + S) = \kappa_y(s)$ , including the case where  $\kappa_{x\text{sf}} \neq \kappa_{y\text{sf}}$ . As one example, for the periodic focusing quadrupole field described by Eqs. (11) and (12) with  $\kappa_x(s) = -\kappa_y(s) \equiv \kappa_q(s)$ ,  $\kappa_q(s + S) = \kappa_q(s)$ , and  $\int_{s_0}^{s_0+S} ds \kappa_q(s) = 0$ , it follows that

$$\bar{\kappa}_x = 0 = \bar{\kappa}_y, \quad \kappa_{x\text{sf}} = \kappa_{y\text{sf}} \equiv \kappa_{\text{sf}}^q, \quad (48)$$

where  $\kappa_{\text{sf}}^q$  is defined by

$$\kappa_{\text{sf}}^q \equiv \left\langle \left( \int_{s_0}^s ds \kappa_q(s) - \left\langle \int_{s_0}^s ds \kappa_q(s) \right\rangle \right)^2 \right\rangle. \quad (49)$$

If  $\kappa_q(s)$  has the form of the step-function lattice with constant amplitude  $\hat{\kappa}_q$  and filling factor  $\eta$ , shown in Fig. 1(a), then it follows from Eq. (49) that [44]

$$\kappa_{\text{sf}}^q = \frac{1}{16} \eta^2 \hat{\kappa}_q^2 S^2 \left( 1 - \frac{2}{3} \eta \right). \quad (50)$$

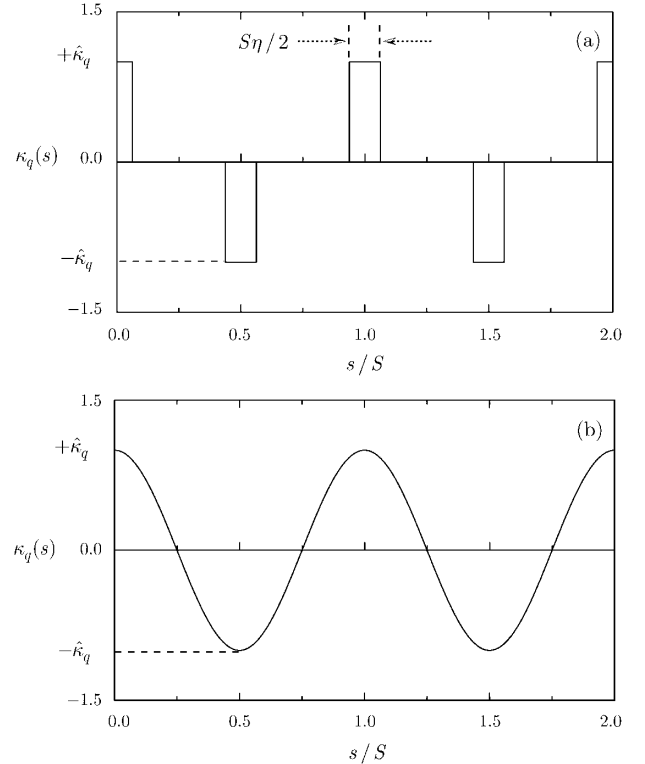


FIG. 1. Examples of a periodic focusing quadrupole lattice  $\kappa_q(s + S) = \kappa_q(s)$  satisfying Eqs. (11) and (12). In (a)  $\kappa_q(s)$  corresponds to a periodic step-function lattice with amplitude  $\hat{\kappa}_q = \text{const}$  and fill factor  $\eta$ . In (b)  $\kappa_q(s) = \hat{\kappa}_q \cos(2\pi s/S)$ , where  $\hat{\kappa}_q = \text{const}$  is the amplitude.

On the other hand, for a sinusoidal lattice function with  $\kappa_q(s) = \hat{\kappa}_q \cos(2\pi s/S)$ , where  $\hat{\kappa}_q = \text{const}$ , as shown in Fig. 1(b), it follows from Eq. (49) that [44]

$$\kappa_{\text{sf}}^q = \frac{1}{2} \frac{\hat{\kappa}_q^2 S^2}{(2\pi)^2}. \quad (51)$$

Note from Eqs. (50) and (51) that  $\kappa_{\text{sf}}^q$  tends to scale as  $\hat{\kappa}_q^2 S^2$  times a factor that depends on the waveform of the lattice function  $\kappa_q(s)$ . As a second example, for the periodic focusing solenoidal field described by Eqs. (13) and (14) with  $\kappa_x(s) = \kappa_y(s) \equiv \kappa_z(s)$ ,  $\kappa_z(s+S) = \kappa_z(s)$ , and  $\bar{\kappa}_z = S^{-1} \int_{s_0}^{s_0+S} ds \kappa_z(s)$ , it follows that

$$\bar{\kappa}_x = \bar{\kappa}_y = \bar{\kappa}_z, \quad \kappa_{x \text{ sf}} = \kappa_{y \text{ sf}} \equiv \kappa_{\text{sf}}^{\text{sol}}, \quad (52)$$

where  $\kappa_{\text{sf}}^{\text{sol}}$  is defined by

$$\kappa_{\text{sf}}^{\text{sol}} \equiv \bar{\kappa}_z + \left\langle \left( \int_{s_0}^s ds \delta \kappa_z(s) - \left\langle \int_{s_0}^s ds \delta \kappa_z(s) \right\rangle \right)^2 \right\rangle. \quad (53)$$

Closed expressions for  $\kappa_{\text{sf}}^{\text{sol}}$  can similarly be determined for various choices of lattice function  $\kappa_z(s+S) = \kappa_z(s)$ .

#### IV. GUIDING-CENTER VLASOV-MAXWELL EQUATIONS

The guiding-center orbit equations (46) and (47) include both the average effects of the applied focusing field (the acceleration terms proportional to  $-\kappa_{x \text{ sf}} \bar{x}$  and  $-\kappa_{y \text{ sf}} \bar{y}$ ) and the average effects of the self-generated fields produced by the beam space charge and axial current (the terms proportional to  $-\partial \bar{\psi} / \partial \bar{x}$  and  $-\partial \bar{\psi} / \partial \bar{y}$ ). Indeed, Eqs. (46) and (47) can be used to derive the corresponding Vlasov-Maxwell equations that describe the self-consistent nonlinear evolution of the guiding-center distribution function  $\bar{f}_b(\bar{x}, \bar{y}, \bar{x}', \bar{y}', s)$  and self-field potential  $\bar{\psi}(\bar{x}, \bar{y}, s)$  in the four-dimensional phase space  $(\bar{x}, \bar{y}, \bar{x}', \bar{y}')$ . We first note that the Hamiltonian  $H_{\perp}(\bar{x}, \bar{y}, \bar{x}', \bar{y}', s)$  describing the transverse guiding-center motion in Eqs. (46) and (47) is given by

$$H_{\perp} = \frac{1}{2}(\bar{x}'^2 + \bar{y}'^2) + \frac{1}{2}[\kappa_{x \text{ sf}} \bar{x}^2 + \kappa_{y \text{ sf}} \bar{y}^2] + \bar{\psi}(\bar{x}, \bar{y}, s), \quad (54)$$

where  $\bar{x}' = d\bar{x}/ds$  and  $\bar{y}' = d\bar{y}/ds$  denote the transverse components of guiding-center velocity. From Eq. (54), it follows that the transverse orbit equations for  $\bar{x}$  and  $\bar{y}$  are given by

$$\begin{aligned} \frac{d\bar{x}}{ds} &= \frac{\partial H_{\perp}}{\partial \bar{x}'} = \bar{x}', \\ \frac{d\bar{x}'}{ds} &= -\frac{\partial H_{\perp}}{\partial \bar{x}} = -\left( \kappa_{x \text{ sf}} \bar{x} + \frac{\partial \bar{\psi}}{\partial \bar{x}} \right), \end{aligned} \quad (55)$$

and

$$\begin{aligned} \frac{d\bar{y}}{ds} &= \frac{\partial H_{\perp}}{\partial \bar{y}'} = \bar{y}', \\ \frac{d\bar{y}'}{ds} &= -\frac{\partial H_{\perp}}{\partial \bar{y}} = -\left( \kappa_{y \text{ sf}} \bar{y} + \frac{\partial \bar{\psi}}{\partial \bar{y}} \right), \end{aligned} \quad (56)$$

which reduce directly to the orbit equations in Eqs. (46) and (47). Of course, the orbit equations in Eqs. (55) and (56) are the characteristics of the nonlinear Vlasov equation for the guiding-center distribution function  $\bar{f}_b(\bar{x}, \bar{y}, \bar{x}', \bar{y}', s)$  in the four-dimensional phase space  $(\bar{x}, \bar{y}, \bar{x}', \bar{y}')$ . Therefore,  $\bar{f}_b(\bar{x}, \bar{y}, \bar{x}', \bar{y}', s)$  evolves according to

$$\begin{aligned} \frac{\partial \bar{f}_b}{\partial s} + \bar{x}' \frac{\partial \bar{f}_b}{\partial \bar{x}} + \bar{y}' \frac{\partial \bar{f}_b}{\partial \bar{y}} - \\ \left( \kappa_{x \text{ sf}} \bar{x} + \frac{\partial \bar{\psi}}{\partial \bar{x}} \right) \frac{\partial \bar{f}_b}{\partial \bar{x}'} - \\ \left( \kappa_{y \text{ sf}} \bar{y} + \frac{\partial \bar{\psi}}{\partial \bar{y}} \right) \frac{\partial \bar{f}_b}{\partial \bar{y}'} = 0. \end{aligned} \quad (57)$$

Here, the self-field potential  $\bar{\psi}(\bar{x}, \bar{y}, s)$  solves Poisson's equation

$$\left( \frac{\partial^2}{\partial \bar{x}^2} + \frac{\partial^2}{\partial \bar{y}^2} \right) \bar{\psi} = -\frac{2\pi K_b}{N_b} \int d\bar{x}' d\bar{y}' \bar{f}_b, \quad (58)$$

where  $K_b$  is the self-field perveance defined in Eq. (2),  $n_b(\bar{x}, \bar{y}, s) = \int d\bar{x}' d\bar{y}' \bar{f}_b(\bar{x}, \bar{y}, \bar{x}', \bar{y}', s)$  is the number density of beam particles, and  $N_b = \int d\bar{x} d\bar{y} n_b(\bar{x}, \bar{y}, s) = \text{const}$  is the number of beam particles per unit axial length.

Equations (57) and (58) constitute the final form of the guiding-center Vlasov-Maxwell equations and can be used to describe the average properties of intense beam propagation through a periodic focusing lattice for a wide range of distribution functions and choices of lattice functions. The range of validity of Eqs. (57) and (58) is similar to the range of validity of the guiding-center orbit equations (46) and (47) derived in Sec. III. That is, Eqs. (57) and (58) are valid to leading order in  $\Delta$  [Eq. (24)] and describe the slow nonlinear evolution of the distribution function  $\bar{f}_b(\bar{x}, \bar{y}, \bar{x}', \bar{y}', s)$  and self-field potential  $\bar{\psi}(\bar{x}, \bar{y}, s)$  over axial length scales long in comparison with the lattice period  $S$ . Information on the (fast) oscillation length scale  $S$ , of course, has been lost in the averaging procedure leading to Eqs. (57) and (58). Nonetheless, there is an enormous amount of information contained in Eqs. (57) and (58) on the detailed equilibrium and stability properties of intense beam propagation over large distances. Furthermore, because the focusing coefficients in Eq. (57) are both constant ( $s$  independent) and positive ( $\kappa_{x \text{ sf}} > 0$  and  $\kappa_{y \text{ sf}} > 0$ ), corresponding to an average inward focusing force, a detailed analysis of the guiding-center Vlasov-Maxwell equations (57) and (58) is far more tractable than an analysis of the original Vlasov-Maxwell equations (7) and (8).

Smooth-focusing Vlasov-Maxwell equations similar to Eqs. (57) and (58) are widely used in the accelerator physics literature [14], most often without a systematic justification, to describe the nonlinear dynamics and collective properties of intense beam propagation. While the primary purpose of this paper is to place Eqs. (57) and (58) on a rigorous, yet physically intuitive, foundation, for completeness we briefly summarize below several general properties of Eqs. (57) and (58) that have important practical consequences.

### A. Intense beam equilibria

The guiding-center Vlasov-Maxwell equations (57) and (58) support a broad class of quasisteady equilibrium solutions with  $\partial/\partial s = 0$ . For example, specializing to the symmetric case with

$$\kappa_{x\text{sf}} = \kappa_{y\text{sf}} \equiv \kappa_{\text{sf}}, \quad (59)$$

Eqs. (57) and (58) support azimuthally symmetric equilibrium solutions ( $\partial/\partial\theta = 0$  and  $\partial/\partial s = 0$ ) for distribution functions  $\bar{f}_b^0(\bar{r}, \bar{x}', \bar{y}')$  of the form [1,36]

$$\bar{f}_b^0 = \bar{f}_b^0(H_\perp^0). \quad (60)$$

Here,

$$H_\perp^0 = \frac{1}{2}(\bar{x}'^2 + \bar{y}'^2) + \frac{1}{2}\kappa_{\text{sf}}\bar{r}^2 + \bar{\psi}^0(\bar{r}) \quad (61)$$

is the ( $s$ -independent) Hamiltonian in the equilibrium field configuration,  $\bar{r} = (\bar{x}^2 + \bar{y}^2)^{1/2}$  is the radial distance from the beam axis, and we have introduced cylindrical polar coordinates  $\bar{x} = \bar{r} \cos\theta$  and  $\bar{y} = \bar{r} \sin\theta$ . In Eqs. (60) and (61), for  $\partial/\partial\theta = 0$ , the equilibrium self-field potential  $\bar{\psi}^0(\bar{r})$  is determined self-consistently in terms of  $\bar{f}_b^0(H_\perp^0)$  from Poisson's equation (58), i.e.,

$$\frac{1}{\bar{r}} \frac{\partial}{\partial \bar{r}} \bar{r} \frac{\partial}{\partial \bar{r}} \bar{\psi}^0(\bar{r}) = \frac{-2\pi K_b}{N_b} \int d\bar{x}' d\bar{y}' \bar{f}_b^0(H_\perp^0). \quad (62)$$

Equations (60)–(62) can be used to investigate detailed equilibrium properties for a wide variety of choices of self-consistent equilibrium distribution function  $\bar{f}_b^0(H_\perp^0)$  [1,36]. Note that Eqs. (60)–(62) contain the full influence of equilibrium self-field effects, and, depending on the choice of distribution function  $\bar{f}_b^0(H_\perp^0)$ , Poisson's equation (62) is generally a nonlinear differential equation for the self-field potential  $\bar{\psi}^0(\bar{r})$ . It is important to note that the class of guiding-center beam equilibria described by Eqs. (59)–(62) has a circular cross section.

### B. Equilibrium radial force balance

We introduce the equilibrium root-mean-square beam radius  $r_{b0}$  and unnormalized transverse emittance  $\epsilon_0$  defined by

$$\begin{aligned} r_{b0}^2 &\equiv \langle \bar{x}^2 + \bar{y}^2 \rangle_0, \\ \epsilon_0^2 &\equiv 4[\langle \bar{x}^2 + \bar{y}^2 \rangle_0 \langle \bar{x}'^2 + \bar{y}'^2 \rangle_0 - \langle \bar{x}\bar{x}' + \bar{y}\bar{y}' \rangle_0^2]. \end{aligned} \quad (63)$$

Here,  $\langle \chi \rangle_0 \equiv N_b^{-1} \int d\bar{x} d\bar{y} d\bar{x}' d\bar{y}' \chi \bar{f}_b^0$  denotes the statistical average of a phase function  $\chi$  over the equilibrium distribution  $\bar{f}_b^0(H_\perp^0)$ , and  $\langle \bar{x}\bar{x}' + \bar{y}\bar{y}' \rangle_0 = 0$  for the class of beam equilibria described by Eqs. (60)–(62). Without presenting algebraic details [1,36], the radial force balance equation,

$$\left( \kappa_{\text{sf}} - \frac{K_b}{2r_{b0}^2} \right) r_{b0} = \frac{\epsilon_0^2}{4r_{b0}^3}, \quad (64)$$

is an exact consequence of the steady-state Vlasov-Maxwell equations for the entire class of self-consistent beam equilibria described by Eqs. (60)–(62). That is, Eq. (64) is valid whatever the choice of equilibrium distribution function  $\bar{f}_b^0(H_\perp^0)$  and corresponding form of the equilibrium density profile  $n_b^0(\bar{r}) = \int d\bar{x}' d\bar{y}' \bar{f}_b^0$ . Equation (64) is a simple statement of (average) radial force balance on a fluid element and corresponds to a balance between the inward force of the applied focusing field ( $-\kappa_{\text{sf}} r_{b0}$ ) and the outward forces due to self-field effects ( $+K_b/2r_{b0}$ ) and the average pressure-gradient force ( $+\epsilon_0^2/4r_{b0}^3$ ). Equation (64) is a powerful constraint condition for the class of beam equilibria described by Eqs. (60)–(62). For example, solving Eq. (64) for the equilibrium mean-square beam radius gives

$$r_{b0}^2 = \frac{K_b}{4\kappa_{\text{sf}}} + \left[ \left( \frac{K_b}{4\kappa_{\text{sf}}} \right)^2 + \frac{\epsilon_0^2}{4\kappa_{\text{sf}}} \right]^{1/2}. \quad (65)$$

Equation (65) shows clearly how  $r_{b0}^2$  increases with increasing beam intensity ( $K_b$ ) and emittance ( $\epsilon_0$ ), and decreases with increasing focusing field strength ( $\kappa_{\text{sf}}$ ).

### C. Kinetic stability theorem

Detailed stability properties can be calculated for the class of beam equilibria described by Eqs. (60)–(62). A small-amplitude stability analysis proceeds by linearizing Eqs. (57) and (58) for perturbations about the equilibrium distribution function  $\bar{f}_b^0(H_\perp^0)$  and corresponding self-field potential  $\bar{\psi}^0(\bar{r})$ , and determining the evolution of the perturbations  $\delta \bar{f}_b(\bar{x}, \bar{y}, \bar{x}', \bar{y}', s)$  and  $\delta \bar{\psi}(\bar{x}, \bar{y}, s)$  [1]. A nonlinear analysis of Eqs. (57) and (58) typically requires implementation of numerical simulation techniques such as the nonlinear perturbative simulation method developed by Qin *et al.* for intense beam applications [1,29]. Direct calculations of detailed stability properties from Eqs. (57) and (58) are typically difficult, but there is a powerful stability theorem that can be demonstrated analytically [27,28]. In particular, for perturbations about the general class of beam equilibria  $\bar{f}_b^0(H_\perp^0)$ , it can be shown [27,28] that a sufficient condition for stability is that the equilibrium distribution function be a monotonically decreasing function of energy  $H_\perp^0$ , i.e.,

$$\frac{\partial}{\partial H_\perp^0} \bar{f}_b^0(H_\perp^0) \leq 0. \quad (66)$$

Whenever Eq. (66) is satisfied, the perturbations  $\delta\tilde{f}_b$  and  $\delta\tilde{\psi}$  do not grow, but rather damp or remain oscillatory. The stability theorem in Eq. (66) is a very powerful result, and is valid nonlinearly (finite-amplitude perturbations) as well as for small-amplitude perturbations. For example, the stability theorem in Eq. (66) implies that a beam with thermal equilibrium distribution [Eq. (67)] is stable and can propagate quiescently over large distances. On the other hand, a Kapchinskij-Vladimirskij distribution [Eq. (68)] has an inverted population in  $H_\perp^0$ , thereby violating Eq. (66), and there is, in principle, free energy available to cause the perturbations  $\delta\tilde{f}_b$  and  $\delta\tilde{\psi}$  to amplify. Both of these important conclusions are validated by numerical simulations [1,29].

#### D. Examples of self-consistent beam equilibria

As noted earlier, Eqs. (60)–(62) can be used to investigate detailed equilibrium properties for a wide variety of self-consistent equilibrium distributions  $\tilde{f}_b^0(H_\perp^0)$  [1,36]. Several choices of  $\tilde{f}_b^0(H_\perp^0)$  are discussed in the literature, and for our purposes here, we simply summarize three illustrative examples. Without loss of generality, we choose  $\tilde{\psi}^0(\bar{r} = 0) = 0$  and  $\tilde{\psi}^0(\bar{r} = r_w) = \psi_w^0 = \text{const}$  consistent with the boundary condition at the conducting wall in Eq. (9). In particular, we consider the following choices of  $\tilde{f}_b^0(H_\perp^0)$  corresponding to the *thermal equilibrium* distribution [1,20,21,23],

$$\tilde{f}_b^0(H_\perp^0) = \hat{n}_b \left( \frac{\gamma_b m_b \beta_b^2 c^2}{2\pi \hat{T}_{\perp b}} \right) \exp \left\{ - \frac{\gamma_b m_b \beta_b^2 c^2}{\hat{T}_{\perp b}} H_\perp^0 \right\}, \quad (67)$$

the *Kapchinskij-Vladimirskij equilibrium* [1,12–16,23],

$$\tilde{f}_b^0(H_\perp^0) = \frac{\hat{n}_b}{2\pi} \delta(H_\perp^0 - \hat{T}_{\perp b} / \gamma_b m_b \beta_b^2 c^2), \quad (68)$$

and the *waterbag equilibrium* [1,18,19,23],

$$\tilde{f}_b^0(H_\perp^0) = \hat{n}_b \left( \frac{\gamma_b m_b \beta_b^2 c^2}{2\pi \hat{T}_{\perp b}} \right) U \left( \frac{\gamma_b m_b \beta_b^2 c^2}{\hat{T}_{\perp b}} H_\perp^0 \right), \quad (69)$$

where  $H_\perp^0 = (1/2)(\bar{x}'^2 + \bar{y}'^2) + (1/2)\kappa_{\text{sf}}\bar{r}^2 + \psi^0(\bar{r})$  is defined in Eq. (61), and  $U(x)$  is the unit step function defined by  $U(x) = +1$  for  $0 \leq x < 1$  and  $U(x) = 0$  for  $x > 1$ . In Eqs. (67)–(69),  $\hat{n}_b$  and  $\hat{T}_{\perp b}$  are positive constants, where  $T_{\perp b}$  has units of energy, and  $\hat{n}_b = n_b^0(\bar{r} = 0)$  is the on-axis number density of beam particles. In Eq. (67),  $\hat{T}_{\perp b} = (\epsilon_0^2/8r_{b0}^2)\gamma_b m_b \beta_b^2 c^2$  can be identified with the uniform kinetic temperature in thermal equilibrium, whereas in Eq. (68)  $\hat{T}_{\perp b} = (\epsilon_0^2/4r_{b0}^2)\gamma_b m_b \beta_b^2 c^2 = T_{\perp b}^0(\bar{r} = 0)$  can be identified with the on-axis transverse temperature of the beam particles. For all three distribution functions in Eqs. (67)–(69), the rms beam radius ( $r_{b0}$ ), the focusing field strength ( $\kappa_{\text{sf}}$ ), the self-field perveance ( $K_b$ ), and the transverse emittance ( $\epsilon_0$ ) are related by the radial force balance constraint in Eq. (64), or equivalently, Eq. (65).

As would be expected, detailed equilibrium properties, such as the density profile  $n_b^0(\bar{r}) = \int d\bar{x}' d\bar{y}' \tilde{f}_b^0(H_\perp^0)$ , are markedly different for the different choices of distribution function in Eqs. (67)–(69) [1]. For example, the density profile calculated from Eq. (67) is generally bell shaped and diffuse, assuming a maximum value ( $\hat{n}_b$ ) at  $\bar{r} = 0$  and decreasing monotonically to zero as  $\bar{r} \rightarrow \infty$ . At low beam intensity and moderate emittance ( $K_b/2 \ll \kappa_{\text{sf}} r_{b0}^2 \approx \epsilon_0^2/4r_{b0}^2$ ), Eqs. (62) and (67) give approximately a Gaussian density profile with  $n_b^0(\bar{r}) \approx \hat{n}_b \exp(-\bar{r}^2/r_{b0}^2)$ . At high beam intensity and low emittance ( $K_b/2 \approx \kappa_{\text{sf}} r_{b0}^2 \gg \epsilon_0^2/4r_{b0}^2$ ), however, Eqs. (62) and (67) give approximately a flattop density profile with  $n_b^0(\bar{r}) \approx \hat{n}_b = \text{const}$ , for  $0 \leq \bar{r} \leq \sqrt{2} r_{b0}$ , which falls abruptly to zero over a few Debye lengths  $\lambda_D \equiv (\gamma_b^2 \hat{T}_{\perp b} / 4\pi \hat{n}_b e_b^2)^{1/2}$  at the beam edge ( $\bar{r} \approx \sqrt{2} r_{b0}$ ). By contrast, for arbitrary values of beam intensity ( $K_b$ ) and emittance ( $\epsilon_0$ ) consistent with Eq. (64), the Kapchinskij-Vladimirskij distribution in Eq. (68) gives (exactly) a step-function density profile with  $n_b^0(\bar{r}) = \hat{n}_b = \text{const}$  in the beam interior ( $0 \leq \bar{r} < \sqrt{2} r_{b0}$ ), and  $n_b^0(\bar{r}) = 0$  for  $\bar{r} > \sqrt{2} r_{b0}$ . Finally, the waterbag equilibrium in Eq. (69) gives a bell-shaped density profile for  $n_b^0(\bar{r})$ , which decreases monotonically to zero for increasing values of  $\bar{r}$ . An important difference between the equilibrium distributions in Eqs. (67) and (69), however, is that the density profile  $n_b^0(\bar{r})$  corresponding to the waterbag equilibrium in Eq. (69) can be calculated in closed analytical form [1], and the beam has a “sharp” outer edge at  $r = \hat{r}_{b0}$  determined self-consistently from

$$I_0(\hat{r}_{b0}/\lambda_D) = \frac{1}{1 - s_b}. \quad (70)$$

Here,  $\lambda_D = (\gamma_b^2 \hat{T}_{\perp b} / 4\pi \hat{n}_b e_b^2)^{1/2}$  is the effective Debye length, and  $s_b < 1$  is the normalized beam intensity defined by  $s_b \equiv \hat{\omega}_{pb}^2 / 2\gamma_b^2 \omega_{\beta\perp}^2$ . Here,  $\hat{\omega}_{pb} \equiv (4\pi \hat{n}_b e_b^2 / \gamma_b m_b)^{1/2}$  is the on-axis relativistic plasma frequency, and  $\omega_{\beta\perp} \equiv (\kappa_{\text{sf}} \beta_b^2 c^2)^{1/2}$  is the transverse focusing frequency associated with the (smooth-focusing) lattice coefficient  $\kappa_{\text{sf}}$ . The preceding is a very brief summary of selected equilibrium properties associated with the distribution functions in Eqs. (67)–(69). Of course, as noted earlier, the stability properties of the beam equilibria described by Eqs. (67)–(69) can be markedly different.

#### V. RANGE OF VALIDITY OF THE GUIDING-CENTER MODEL

The analysis leading to the guiding-center orbit equations (46) and (47), and the corresponding Vlasov-Maxwell equations for  $\tilde{f}_b(\bar{x}, \bar{y}, \bar{x}', \bar{y}', s)$  and  $\tilde{\psi}(\bar{x}, \bar{y}, s)$  in Eqs. (57) and (58), is, of course, approximate since we have averaged over the (fast) oscillations occurring on the length scale  $S$  of the lattice period. As indicated earlier, validity of such a guiding-center

model requires sufficiently small phase advance  $\sigma$ , or, equivalently, sufficiently small values of the parameter  $\sqrt{\kappa_{x\text{sf}}} S/2\pi \sim \sqrt{\kappa_{y\text{sf}}} S/2\pi \sim \Delta$  [Eq. (24)]. To assess the range of validity of the guiding-center model, we consider the particular example of a Kapchinskij-Vladimirskij distribution function  $f_b^{\text{KV}}(x, y, x', y', s)$  [43], which provides an exact periodically focused solution to the full Vlasov-Maxwell equations (7) and (8). We further assume a periodic quadrupole lattice with  $\kappa_x(s) = -\kappa_y(s) \equiv \kappa_q(s)$  [Eq. (11)] with  $\kappa_q(s + S) = \kappa_q(s)$  and  $\int_{s_0}^{s_0+S} ds \kappa_q(s) = 0$ . Without presenting algebraic details, the corresponding density profile  $n_b(x, y, s) = \int dx' dy' f_b^{\text{KV}}$  can be expressed as [43]

$$n_b(x, y, s) = \begin{cases} \frac{N_b}{\pi ab}, & 0 \leq x^2/a^2 + y^2/b^2 < 1, \\ 0, & x^2/a^2 + y^2/b^2 > 1, \end{cases} \quad (71)$$

and the self-field potential in the beam interior is given by [43]

$$\psi(x, y, s) = -\frac{K_b}{a+b} \left[ \frac{1}{a} x^2 + \frac{1}{b} y^2 \right], \quad (72)$$

for  $0 \leq x^2/a^2(s) + y^2/b^2(s) < 1$ . Note from Eq. (71) that the density profile  $n_b(x, y, s) = N_b/\pi ab$  is uniform within the pulsating elliptical cross section  $x^2/a^2(s) + y^2/b^2(s) = 1$ . Moreover, the envelope equations for the ellipse dimensions,  $a(s)$  and  $b(s)$ , are given by [1]

$$\frac{d^2}{ds^2} a + \left[ \kappa_q(s) - \frac{2K_b}{a(a+b)} \right] a = \frac{\epsilon^2}{a^3}, \quad (73)$$

$$\frac{d^2}{ds^2} b + \left[ -\kappa_q(s) - \frac{2K_b}{b(a+b)} \right] b = \frac{\epsilon^2}{b^3}, \quad (74)$$

where we have assumed  $\epsilon_x^2 = \epsilon_y^2 = \epsilon^2$ . Substituting Eq. (72) into the orbit equations (19) and (20) gives

$$\frac{d^2}{ds^2} x + \left[ \kappa_q(s) - \frac{2K_b}{a(a+b)} \right] x = 0, \quad (75)$$

$$\frac{d^2}{ds^2} y + \left[ -\kappa_q(s) - \frac{2K_b}{b(a+b)} \right] y = 0, \quad (76)$$

which can be used to determine the exact particle trajectories  $x(s)$  and  $y(s)$ . In Eqs. (75) and (76), note that  $a(s)$  and  $b(s)$  are determined self-consistently from the envelope equations (73) and (74).

On the other hand, for the axisymmetric guiding-center Kapchinskij-Vladimirskij equilibrium in Eq. (68), the self-field potential within the uniform density beam is given by  $\bar{\psi}^0(\bar{r}) = -(1/4)K_b \bar{r}^2/r_{b0}^2$ , where

$$\bar{a} = \bar{b} = \sqrt{2} r_{b0} \quad (77)$$

is the outer envelope of the (average) beam cross section, and the rms beam radius  $r_{b0}$  is determined self-consistently from the radial force balance equation (64), or equivalently,

Eq. (65). Substituting  $\bar{\psi}^0(\bar{r})$  into Eqs. (46) and (47), we obtain

$$\frac{d^2}{ds^2} \bar{x} + \left[ \kappa_{\text{sf}}^q - \frac{K_b}{2r_{b0}^2} \right] \bar{x} = 0, \quad (78)$$

$$\frac{d^2}{ds^2} \bar{y} + \left[ \kappa_{\text{sf}}^q - \frac{K_b}{2r_{b0}^2} \right] \bar{y} = 0, \quad (79)$$

which determines the (slow) evolution of the guiding-center orbits  $\bar{x}(s)$  and  $\bar{y}(s)$ . Here  $\kappa_{\text{sf}}^q = \text{const}$  is defined in Eq. (49) for general periodic quadrupole lattice  $\kappa_q(s + S) = \kappa_q(s)$ . The coefficients in Eqs. (78) and (79) are constant (independent of  $s$ ), and the solutions are simple combinations of  $\cos[(\kappa_{\text{sf}}^q - K_b/2r_{b0}^2)^{1/2}s]$  and  $\sin[(\kappa_{\text{sf}}^q - K_b/2r_{b0}^2)s]$ . By contrast, the (oscillatory) coefficients in the orbit equations (75) and (76) are  $s$  dependent, and it is most convenient to solve Eqs. (75) and (76) numerically for the particle orbits  $x(s)$  and  $y(s)$ .

As an illustrative numerical example, we consider the step-function quadrupole lattice illustrated in Fig. 1(a) with filling factor  $\eta = 0.25$  and normalized amplitude  $\hat{\kappa}_q S^2 = 9.08$ . Numerical integration of the envelope equations (73) and (74), assuming matched-beam solutions with  $a(s + S) = a(s)$  and  $b(s + S) = b(s)$ , shows that the vacuum phase advance [1] is given by  $\sigma_v = 30^\circ = \pi/6$ , where  $\sigma_v$  is defined by

$$\sigma_v = \lim_{K_b \rightarrow 0} \epsilon \int_{s_0}^{s_0+S} \frac{ds}{a^2(s)} = \lim_{K_b \rightarrow 0} \epsilon \int_{s_0}^{s_0+S} \frac{ds}{b^2(s)}. \quad (80)$$

Periodic solutions to the envelope equations (73) and (74) for the choice of system parameters  $\eta = 0.25$ ,  $\hat{\kappa}_q S^2 = 9.08$ , and  $\sigma_v = 30^\circ = \pi/6$  are shown in Fig. 2. For this choice of parameters, note from Eq. (50) that

$$\kappa_{\text{sf}}^q S^2 = 0.268, \quad (81)$$

which corresponds to  $\sqrt{\kappa_{\text{sf}}^q} S/2\pi = 0.082 = \Delta$  [Eq. (24)]. Two cases are illustrated in Fig. 2, where the normalized beam dimensions,  $a(s)/\sqrt{\epsilon S}$  and  $b(s)/\sqrt{\epsilon S}$ , are plotted versus  $s/S$  for periodic matched-beam solutions to Eqs. (73) and (74). The results in Fig. 2(a) correspond to a very-low-intensity beam with  $2\epsilon S/a^2 \gg K_b S/\epsilon = 0.01$ , whereas the plots shown in Fig. 2(b) correspond to a moderate-intensity beam with  $2\epsilon S/a^2 \sim K_b S/\epsilon = 0.8$ . The total phase advance  $\sigma$  (including space-charge depression) is  $\sigma = 29.7^\circ$  in Fig. 2(a) and  $\sigma = 14.85^\circ$  in Fig. 2(b). From Figs. 2(a) and 2(b), the (numerically determined) average beam envelope dimensions obtained from Eqs. (73) and (74) are found to be  $\bar{a}/\sqrt{\epsilon S} = \bar{b}/\sqrt{\epsilon S} = 1.402$  in Fig. 2(a), and  $\bar{a}/\sqrt{\epsilon S} = \bar{b}/\sqrt{\epsilon S} = 1.983$  in Fig. 2(b). On the other hand, from the guiding-center estimates in Eqs. (65) and (77), we obtain  $\sqrt{2} r_{b0}/\sqrt{\epsilon S} = 1.396$  for the choice of system parameters in Fig. 2(a), and  $\sqrt{2} r_{b0}/\sqrt{\epsilon S} = 1.982$  for the choice of system parameters in Fig. 2(b). Evidently, for the choice of parameters in Fig. 2, the guiding-center model developed in Secs. III and IV provides

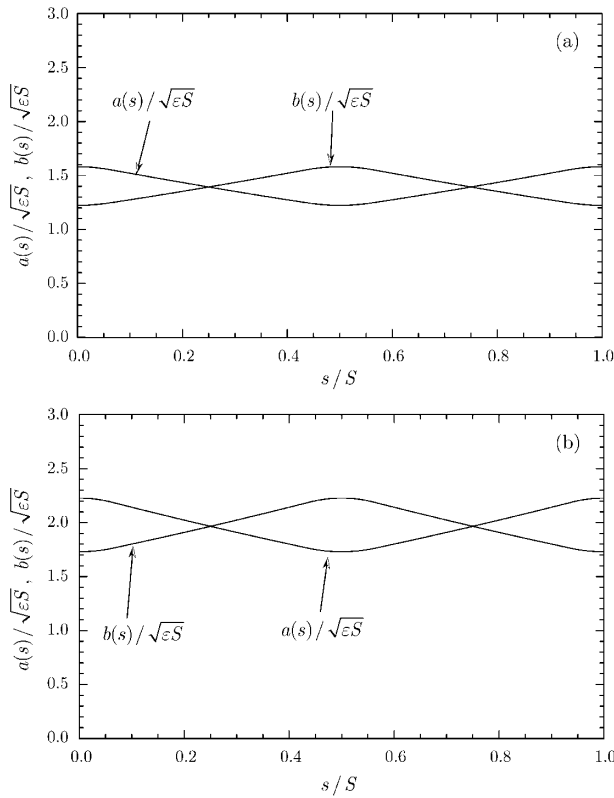


FIG. 2. Matched beam solutions for  $a(s)/\sqrt{\epsilon S}$  and  $b(s)/\sqrt{\epsilon S}$  obtained numerically from Eqs. (73) and (74) are plotted versus  $s/S$  for the step-function lattice in Fig. 1(a) for system parameters corresponding to  $\eta = 0.25$ ,  $\hat{\kappa}_q S^2 = 9.08$  and  $\sigma_v = 30^\circ$ , and normalized beam intensity corresponding to (a)  $K_b S/\epsilon = 0.01$  and  $\sigma = 29.7^\circ$ , and (b)  $K_b S/\epsilon = 0.8$  and  $\sigma = 14.85^\circ$ .

an excellent description of the average transverse beam dimensions, even in the regime of high self-field intensity.

Illustrative solutions to the exact orbit equations (75) and (76) for  $x(s)$  and  $y(s)$ , and the guiding-center orbit equations (78) and (79) for  $\bar{x}(s)$  and  $\bar{y}(s)$  are shown in Fig. 3. Here, the system parameters in Fig. 3(a) are the same as those in Fig. 2(a), and the system parameters in Fig. 3(b) are the same as those in Fig. 2(b). In both cases, we integrate the orbit equations from  $s = s_0 = 0$  to  $s = 60S$ . In Figs. 3(a) and 3(b), the smooth curves without small length-scale variations correspond to plots of  $\bar{x}(s)/\sqrt{\epsilon S}$  versus  $s/S$  determined from Eq. (78) for initial conditions  $\bar{x}_0/\sqrt{\epsilon S} = 0.5\bar{a}/\sqrt{\epsilon S}$  and  $[d\bar{x}/ds]_{s=0} = 0$ , where  $\bar{x}_0 = \bar{x}(s=0)$ . On the other hand, the curves with small length-scale variations in Figs. 3(a) and 3(b) correspond to the numerical solutions to the exact orbit equation (75) for  $x(s)$  for initial conditions corresponding to  $x(s=0) = \bar{x}_0 + \delta x(s=0) = 1.12\bar{x}_0$  and  $[dx/ds]_{s=0} = 0$ . Note from Fig. 3 that  $x(s)$  oscillates (with period  $S$ ) about the average guiding-center orbit  $\bar{x}(s)$ . Indeed, it is clear from Fig. 3 that the guiding-center orbit  $\bar{x}(s)$  calculated from Eq. (78) gives an excellent approximation to the *average* orbit for  $x(s)$  determined from the exact orbit equation (75). This is true for both the

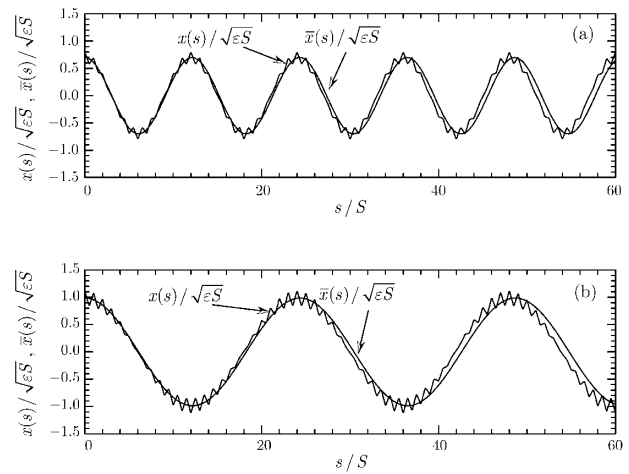


FIG. 3. The solutions for  $x(s)/\sqrt{\epsilon S}$  and  $\bar{x}(s)/\sqrt{\epsilon S}$  obtained from Eqs. (75) and (78) are plotted versus  $s/S$  for the step-function lattice in Fig. 1(a) for system parameters corresponding to  $\eta = 0.25$ ,  $\hat{\kappa}_q S^2 = 9.08$  and  $\sigma_v = 30^\circ$ , and normalized beam intensity corresponding to (a)  $K_b S/\epsilon = 0.01$  and  $\sigma = 29.7^\circ$ , and (b)  $K_b S/\epsilon = 0.8$  and  $\sigma = 14.85^\circ$ . Initial conditions correspond to  $\bar{x}_0 = 0.5\bar{a}/\sqrt{\epsilon S}$  and  $x(s=0) = \bar{x}_0 + \delta x(s=0) = 1.12\bar{x}_0$ .

case of low beam intensity [Fig. 3(a)] and the case of high beam intensity [Fig. 3(b)]. Furthermore, for high beam intensity [Fig. 3(b)], the axial period of the guiding-center orbit  $\bar{x}(s)$  is longer than for the case of low beam intensity [Fig. 3(a)]. For the system parameters in Fig. 3(a), the guiding-center model overestimates the (slow) oscillation wavelength by 1.1%, whereas, in Fig. 3(b), the guiding-center model overestimates the oscillation wavelength by 1.6%.

In Fig. 4, the ratio between the smooth-focusing phase advance  $\sigma_{sf} = (\kappa_{sf}^q - K_b/2r_{b0}^2)^{1/2} S$  [44] and the exact phase advance  $\sigma$  is plotted versus the vacuum phase

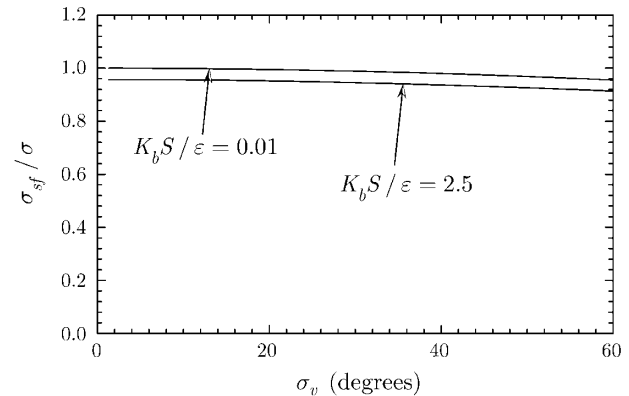


FIG. 4. The ratio between the smooth-focusing phase advance  $\sigma_{sf}$  and the exact phase advance  $\sigma$  is plotted versus the vacuum phase advance  $\sigma_v$  for system parameters  $\eta = 0.25$  and  $0 < \hat{\kappa}_q S^2 < 21.5$ . The upper and lower curves correspond to the low and high space-charge cases with  $K_b S/\epsilon = 0.01$  and  $K_b S/\epsilon = 2.5$ , respectively.

advance  $\sigma_v$  for system parameters corresponding to  $\eta = 0.25$ . The variation domain of the vacuum phase advance is  $0^\circ < \sigma_v < 60^\circ$ , corresponding to  $0 < \hat{\kappa}_q S^2 < 21.5$ . As evident from the plot, the error in phase advance introduced by the smooth-focusing guiding-center model is less than 9% for both the low and the high space-charge cases corresponding to  $K_b S/\epsilon = 0.01$  and  $K_b S/\epsilon = 2.5$ , respectively.

## VI. CONCLUSIONS

In this paper, we provided a systematic derivation of a guiding-center kinetic model that describes intense beam propagation through a periodic focusing lattice with axial periodicity length  $S$ , valid for sufficiently small phase advance (say,  $\sigma < 60^\circ$ ). The analysis assumed a thin ( $a, b \ll S$ ) axially continuous beam, or very long charge bunch, propagating in the  $z$  direction through a periodic focusing lattice with transverse focusing coefficients  $\kappa_x(s + S) = \kappa_x(s)$  and  $\kappa_y(s + S) = \kappa_y(s)$ , where  $S = \text{const}$  is the lattice period (Sec. II). By averaging over the (fast) oscillations occurring on the length scale of a lattice period  $S$  (Sec. III), the analysis led to the *smooth-focusing* Vlasov-Maxwell equations (57) and (58) (Sec. IV) that describe the slow evolution of the guiding-center distribution function  $\bar{f}_b(\bar{x}, \bar{y}, \bar{x}', \bar{y}', s)$  and (normalized) self-field potential  $\bar{\psi}(\bar{x}, \bar{y}, s)$  in the four-dimensional transverse phase space  $(\bar{x}, \bar{y}, \bar{x}', \bar{y}')$ . In the resulting kinetic equation (57) for  $\bar{f}_b(\bar{x}, \bar{y}, \bar{x}', \bar{y}', s)$ , the average effects of the applied focusing field are incorporated in the *constant* focusing coefficients  $\kappa_{x\text{sf}} > 0$  and  $\kappa_{y\text{sf}} > 0$  defined in Eqs. (44) and (45), and the model is readily accessible to direct analytical investigation. Similar smooth-focusing Vlasov-Maxwell descriptions are widely used in the accelerator physics literature, often without a systematic justification, and the present analysis places these models on a rigorous, yet physically intuitive, foundation.

## ACKNOWLEDGMENTS

This research was supported by the Department of Energy and in part by the Office of Naval Research.

- [1] R. C. Davidson and H. Qin, *Physics of Intense Charged Particle Beams in High Energy Accelerators* (World Scientific, Singapore, 2001).
- [2] T. P. Wangler, *Principles of RF Linear Accelerators* (Wiley, New York, 1998).
- [3] A. W. Chao, *Physics of Collective Beam Instabilities in High Energy Accelerators* (Wiley, New York, 1993).
- [4] M. Reiser, *Theory and Design of Charged Particle Beams* (Wiley, New York, 1994).
- [5] S. Y. Lee, *Accelerator Physics* (World Scientific, Singapore, 1999).
- [6] H. Wiedemann, *Particle Accelerator Physics II: Nonlinear and Higher-Order Beam Dynamics* (Springer-Verlag, New York, 1998).
- [7] H. Wiedemann, *Particle Accelerator Physics I: Basic Principles and Linear Beam Dynamics* (Springer-Verlag, New York, 1999).
- [8] D. A. Edwards and M. J. Syphers, *An Introduction to the Physics of High Energy Accelerators* (Wiley, New York, 1993).
- [9] J. D. Lawson, *The Physics of Charged Particle Beams* (Oxford Science Publications, New York, 1988).
- [10] See, for example, *Proceedings of the 1999 Particle Accelerator Conference, New York* (IEEE, Piscataway, NJ, 1999), pp. 1–3778.
- [11] See, for example, *Proceedings of the International Heavy Ion Fusion Symposium* [Nucl. Instrum. Methods Phys. Res., Sect. A **464**, 1–674 (2001)].
- [12] I. M. Kapchinskij and V. V. Vladimirkij, in *Proceedings of the International Conference on High Energy Accelerators and Instrumentation* (CERN, Geneva, 1959), p. 274.
- [13] R. L. Gluckstern, in *Proceedings of the 1970 Proton Linear Accelerator Conference, Batavia, IL*, edited by M. R. Tracy (National Accelerator Laboratory, Batavia, IL, 1971), p. 811.
- [14] See, for example, Chaps. 4–8 of Ref. [1], and references therein.
- [15] T.-S. Wang and L. Smith, Part. Accel. **12**, 247 (1982).
- [16] I. Hofmann, L. J. Laslett, L. Smith, and I. Haber, Part. Accel. **13**, 145 (1983).
- [17] J. Struckmeier, J. Klabunde, and M. Reiser, Part. Accel. **15**, 47 (1984).
- [18] I. Hofmann and J. Struckmeier, Part. Accel. **21**, 69 (1987).
- [19] J. Struckmeier and I. Hofmann, Part. Accel. **39**, 219 (1992).
- [20] N. Brown and M. Reiser, Phys. Plasmas **2**, 965 (1995).
- [21] R. C. Davidson and H. Qin, Phys. Rev. ST Accel. Beams **2**, 114401 (1999).
- [22] R. L. Gluckstern, W.-H. Cheng, and H. Ye, Phys. Rev. Lett. **75**, 2835 (1995).
- [23] R. C. Davidson and C. Chen, Part. Accel. **59**, 175 (1998).
- [24] C. Chen, R. Pakter, and R. C. Davidson, Phys. Rev. Lett. **79**, 225 (1997).
- [25] C. Chen and R. C. Davidson, Phys. Rev. E **49**, 5679 (1994).
- [26] R. C. Davidson, W. W. Lee, and P. Stoltz, Phys. Plasmas **5**, 279 (1998).
- [27] R. C. Davidson, Phys. Rev. Lett. **81**, 991 (1998).
- [28] R. C. Davidson, Phys. Plasmas **5**, 3459 (1998).
- [29] H. Qin, R. C. Davidson, and W. W. Lee, Phys. Rev. ST Accel. Beams **3**, 084401 (2000); **3**, 109901 (2000).
- [30] P. H. Stoltz, R. C. Davidson, and W. W. Lee, Phys. Plasmas **6**, 298 (1999).
- [31] W. W. Lee, Q. Qian, and R. C. Davidson, Phys. Lett. A **230**, 347 (1997).
- [32] Q. Qian, W. W. Lee, and R. C. Davidson, Phys. Plasmas **4**, 1915 (1997).
- [33] A. Friedman, D. P. Grote, and I. Haber, Phys. Fluids B **4**, 2203 (1992).
- [34] A. Friedman, J. J. Barnard, D. P. Grote, and I. Haber, Nucl. Instrum. Methods Phys. Res., Sect. A **415**, 455 (1998).
- [35] S. M. Lund, J. J. Barnard, G. D. Craig, A. Friedman, D. P. Grote, H. S. Hopkins, T. S. Sangster, W. M. Sharp, S. Eylon, T. T. Fessenden, E. Henestroza, S. Yu, and I. Haber, Nucl. Instrum. Methods Phys. Res., Sect. A **415**, 345 (1998).
- [36] R. C. Davidson, H. Qin, and P. J. Channell, Phys. Rev. ST Accel. Beams **2**, 074401 (1999); **3**, 029901 (2000).

- 
- [37] P.J. Channell, Phys. Plasmas **6**, 982 (1999).  
[38] R. A. Kishek, P. G. O'Shea, and M. Reiser, Phys. Rev. Lett. **85**, 4514 (2000).  
[39] S. M. Lund and R. C. Davidson, Phys. Plasmas **5**, 3028 (1998).  
[40] R. C. Davidson and S. Strasburg, Phys. Plasmas **7**, 2657 (2000).  
[41] S. Strasburg and R. C. Davidson, Phys. Lett. A **269**, 40 (2000).  
[42] I. Hofmann, Phys. Rev. E **57**, 4713 (1998).  
[43] See, for example, Chap. 5 of Ref. [1].  
[44] See, for example, Sec. 3.5 of Ref. [1].